Carbonate veins trace seawater circulation during exhumation and uplift of mantle rock: Results from ODP Leg 209

Wolfgang Bach
Geoscience Department, University of Bremen, 28359 Bremen, Germany,
wbach@uni-bremen.de (correspondence author, Tel: ++49-421-218-65400)

Martin Rosner[a]
Geoscience Department, University of Bremen, 28359 Bremen, Germany, and
Helmholtz-Zentrum Potsdam Deutsches GeoForschungsZentrum GFZ,
Telegrafenberg, D-14473 Potsdam, Germany

Niels Jöns
Geoscience Department and MARUM, University of Bremen, 28359 Bremen,
Germany, njoens@uni-bremen.de

Svenja Rausch
Geoscience Department, University of Bremen, 28359 Bremen, Germany,
srausch@uni-bremen.de

Laura F. Robinson
Department of Marine Chemistry and Geochemistry, Woods Hole Oceanographic
Institution, Woods Hole, MA 02543, USA, lrobinson@whoi.edu

Holger Paulick[b]
Steinmann Institut, University of Bonn, Universität Bonn, Poppelsdorfer Schloss,
53115 Bonn, Germany

Jörg Erzinger

Helmholtz-Zentrum Potsdam Deutsches GeoForschungsZentrum GFZ,

Telegrafenberg, D-14473 Potsdam, Germany

Submitted to *Earth and Planetary Science Letters*

February 8, 2011

revised version of August 27, 2011

re-revised version of September 2, 2011

[a]Now at: BAM Federal Institute for Materials Research and Testing, Department I. Analytical chemistry; reference materials, Unter den Eichen 87, 12205 Berlin, Germany (martin.rosner@bam.de)

[b]Now at: Boliden Mineral AB, 93681 Boliden, Sweden (Holger.Paulick@Boliden.com)

Abstract

Carbonate veins hosted in ultramafic basement drilled at two sites in the Mid Atlantic Ridge 15°N area record two different stages of fluid-basement interaction. A first generation of carbonate veins consists of calcite and dolomite that formed syn- to postkinematically in tremolite-chlorite schists and serpentine schists that represent gently dipping large-offset faults. These veins formed at temperatures between 90 and 170°C (oxygen isotope thermometry) and from fluids that show intense exchange of Sr and Li with the basement ($^{87}Sr/^{86}Sr$=0.70387 to 0.70641, $\delta^{7}Li_{L\text{-}SVEC}$ = +3.3 to +8.6‰). Carbon isotopic compositions range to high $\delta^{13}C_{PDB}$ values (8.7‰), indicating that methanogenesis took place at depth. The Sr-Li-C isotopic composition suggests temperatures of fluid-rock interaction that are much higher (T>350-400°C) than the temperatures of vein mineral precipitation inferred from oxygen isotopes. A possible explanation for this discrepancy is that fluids cooled conductively during upflow within the presumed detachment fault

Aragonite veins were formed during the last 130 kyrs at low-temperatures within the uplifted serpentinized peridotites. Chemical and isotopic data suggest that the aragonites precipitated from cold seawater, which underwent overall little exchange with the basement. Oxygen isotope compositions indicate an increase in formation temperature of the veins by 8-12°C within the uppermost ~80 m of the subseafloor. This increase corresponds to a high regional geothermal gradient of 100-150°C/km, characteristic of young lithosphere undergoing rapid uplift.

Keywords

hydrothermal processes, seawater circulation, carbonate veining, ocean-crust exchange, Li isotopes, age dating

1. Introduction

Alteration of peridotite by circulation of seawater at slow-spreading mid-ocean ridges (MOR) has profound consequences for the thermal structure and rheology of the oceanic lithosphere, geochemical budgets of the ocean and the atmosphere and microbial processes within and at the seafloor. Carbonate veins are a common low- to moderate-temperature feature in all lithologies of altered ocean lithosphere. Previous studies have shown that the chemical and isotopic composition of these carbonate veins can be used to gain information about the composition and physico-chemical properties of the precipitating fluid and the age of formation (e.g., Bonatti et al., 1980; Früh-Green et al., 2003; Coggon et al., 2004; Eickmann et al., 2009). Most previous studies of carbonates from altered ocean lithosphere were focused on volcanic sections of crust generated at intermediate and fast spreading MORs (Staudigel et al., 1996; Alt and Teagle, 1999; Alt and Teagle, 2003). In these studies, it was proposed that the oceanic crust is an important sink for CO_2 due to the CO_2-uptake during aging, with uptake rates on the order of $2 \cdot 10^{12}$ moles/yr (e.g., Alt and Teagle, 1999). Carbonate veining is about an order of magnitude less abundant in tectonically exhumed lower oceanic crust (Bach et al., 2001). The impact of vein carbonates hosted in ultramafic rocks on the global carbon budget, however, has not yet been assessed. This knowledge gap is critical, as 20-25% of the seafloor created along slow-spreading ridges is ultramafic in composition (Cannat et al., 2010), and ultramafic rocks are potentially important sites of CO_2 sequestration (Kelemen and Matter, 2008).

To estimate carbonate vein abundance and reconstruct the physico-chemical conditions and timing of carbonate precipitation in ultramafic basement we studied carbonate veins from the slow-spreading Mid-Atlantic Ridge (MAR) at 15°20'N, where the basement is dominantly ultramafic for a stretch of about 100km ridge length (Escartin and Cannat, 1999; Kelemen et al., 2007). The combination of trace

element data with Li-C-O-Sr isotope compositions and radiometric age determinations allows unique insights into the chemical and isotopic evolution of seawater within the basement and the timing of carbonate formation during sub-seafloor water-rock interactions. The data are also useful in constraining upward migration of deeply rooted hydrothermal fluids within detachment faults that expose mantle rocks at the seafloor.

2. Geological setting and sample description

The carbonate veins investigated in this study occur in serpentinized harzburgites and dunites and were drilled at the slow-spreading mid-Atlantic ridge (MAR) during ODP Leg 209 at two sites on the western wall of the axial valley north (Site 1274) and south (Site 1271) of the 15°20'N Fracture Zone (Fig. 1). The seafloor at both sites is a smooth fault scarp dipping gently (10°-18°) to the east (Kelemen et al., 2007). Displacement on these faults is >5-6 km and the fault rocks, particular at Site 1271, preserve a history of deformation and alteration from 700°C to ambient temperatures (Schroeder et al., 2007). The fault at Site 1271 was interpreted as a terminated detachment fault that is secondary to active detachment faulting on the eastern valley wall (Schroeder et al., 2007). The semi-brittle deformation manifest in these rocks relates to denudation of the mantle along that presumed detachment fault. The basement at both sites is cut by younger normal faults. Brittle deformation in these faults produced serpentine fault gouge, which is developed in several intervals in Holes 1274A and 1271B. Using a half-spreading rate of 12 km/Myr and the distance between the drill sites and the termination of the detachment fault, the age of the seafloor can be estimated at 0.7 Ma (Site 1274) and 1.5 Ma (Site 1271).

Two carbonate vein types have been distinguished on the basis of structural, mineralogical and compositional criteria (Fig. 2). The first type is calcite (containing

subordinate amounts of dolomite) veins developed only in chlorite-tremolite and serpentine schists from the uppermost basement at Site 1271 (Figs. 2a, 2c, 2d). These veins are abundantly folded and intergrown with serpentine, indicating synkinematic formation. The most abundant and volumetrically dominant (>90%) type is mm- to cm-wide aragonite veins (Figs. 2d, 2e, 2f) that formed during the latest stage of sub-seafloor alteration. Crosscutting relationships indicate that their formation postdates all other vein generations (Shipboard Science Party, 2003; Bach et al., 2004). Aragonite veins are typically bordered by cm-wide reddish to brownish halos with iron-hydroxides, indicating aragonite precipitation from oxygenated seawater. These vein halos are narrow (mm-scale) in cores from Hole 1274A, but wider (cm-scale) and more common in core from the holes at Site 1271 (Fig. 1). The aragonite veins formed during the latest stages of exhumation and uplift, when the basement experienced fracturing and brittle faulting allowing seawater to penetrate and cause aragonite precipitation. Oxidative seawater alteration is limited to the uppermost basement at Site 1274, as aragonite veins and oxidation halos disappear below a fault gouge at 95 m below seafloor (Shipboard Science Party, 2003).

3. Analytical methods

3.1 Li and Sr isotopes

Separates from carbonate veins were collected by handpicking (2 – 20 mg) from crushed core samples. The separates were twice rinsed in water (18.2 MΩ cm) before the carbonate phase was dissolved with suprapure acetic acid. The Li and Sr containing supernatants were separated from un-dissolved non-carbonate phases by centrifugation and split into two aliquots for Sr and Li isotope analyses. Prior to ion-chromatographic Li and Sr separation, the solutions were evaporated to dryness at 70°C on a hotplate. The residues were then re-dissolved in 3 N HNO_3 for Li separation and 2.5 N HCl for Sr separation, and again evaporated to dryness (at 120°C). The Li-matrix separation was carried out on columns

loaded with 10 ml AG 50W X8 cation resin (200-400 mesh; 1.1 cm diameter, 10 cm height) using a HNO_3-MeOH mixture (1 M HNO_3 in 80% v/v MeOH). The Sr-matrix separation was achieved by conventional ion chromatography using 3 ml AG 50W-X8 (200-400 mesh) and 2.5 M HCl.

Sr and Li isotope compositions were determined by MC-ICP-MS on a Thermo Finnigan NEPTUNE at Woods Hole Oceanographic Institution (WHOI) using the methods of Jackson and Hart (2006) and Rosner et al. (2007). The Li isotope composition was determined by static multi-collection on masses 6 and 7 from the separated solutions containing 100 ppb Li. The Li isotope compositions are reported in the conventional δ notation relative to the NIST lithium carbonate SRM 8545 (L-SVEC; Flesch et al., 1973) and were calculated using standard-sample-standard bracketing. Based on the external reproducibility of independently processed sample aliquots and comparison of our data to established δ^7Li values for reference and quality control materials, the overall uncertainty of the presented δ^7Li data can be estimated to be 0.5 ‰ (2σ; Rosner et al., 2007).

The Sr isotope composition was determined by static multi-collection from the separated solutions containing 200 to 800ppb Sr. To correct for Kr and Rb contributions on the raw data, the reduction scheme of Jackson and Hart (2006) was used. Repeated measurements (n = 32) of the isotope reference material NIST SRM® 987 yielded a mean $^{87}Sr/^{86}Sr$ ratio of 0.710244(28) (2σ). The latter value is in good agreement with the accepted value for NBS 987 of 0.71025 (e.g., Banner, 2004) and therefore no further correction for the $^{87}Sr/^{86}Sr$ ratio has been applied.

3.2 Oxygen and carbon isotope analyses

Decomposition of about 10 mg carbonate minerals for mass spectrometric analyses at the University of Bonn was carried out by treatment of the pulverized samples with H_3PO_4 in evacuated glass tubes (McCrea, 1950) at room temperature conditions for approximately 24 h. The O- and C-isotope determinations were carried out on a VG SIRA-9 instrument (triple collector, 90°, 9 cm radius). The results are reported as per mille deviation of the sample from the PDB standard for carbon and from the SMOW standard for oxygen. Multiple duplicate analyses show that the reproducibility of results was better than ±0.1‰. Temperatures were

calculated for aragonite using the calibration of Grossman and Ku (1986), which was validated more recently by Kim et al. (2007). A $\delta^{18}O$ seawater value of 0.22‰ (Shanks, 2001) was assumed. Temperatures of calcite formation were computed using the calibration of Kim and O'Neil (1997).

3.3 Trace element analyses

Approximately 5 mg of carbonate was hand-picked from crushed vein material, wetted with 1 g of water (18.2 MΩ cm), and dissolved upon slow addition of 1 g of 4% nitric acid. Samples were diluted 1:3 with 4% nitric acid and an In spike was added as internal standard. Solutions were measured on a Thermo Finnigan Element2 high-resolution ICP-MS at WHOI, calibrated with six In-spiked standard solutions matrix-matched for Ca-concentrations. Mg, Sr, and Na concentrations were measured in high-resolution mode, the other elements were measured in low-resolution mode. Reproducibility and accuracy were checked by measuring a low concentration standard as unknown. The uncertainties of the concentrations are <5%.

3.4 Radiometric age dating

Four mg of carefully handpicked carbonate vein material was cleaned in acetone and rinsed several times with water (18.2 MΩ cm). The samples were radiocarbon-dated by the National Ocean Sciences Accelerator Mass Spectrometry (NOSAMS) facility at WHOI using procedures outlined in http://www.nosams.whoi.edu/images/amsgenst.pdf. The radiocarbon ages were converted to calendar ages using Intcal04 (Reimer et al., 2010)

Approximately 0.4-1g from each of three samples (two from Hole 1274A and one from Hole 1271B) were crushed into chunks, hand-picked to remove as much visible serpentine as possible, ultrasonicated in milliQ water and dried. Samples were then weighed, dissolved in 8N nitric acid and spiked with a mixed ^{229}Th - ^{236}U spike. U and Th were separated and purified by anion-exchange chemistry (Edwards et al., 1986) and measured by a Neptune MC-ICP-MS using bracketing standards CRM-145 and an in-house Th standard (Robinson et al., 2005).

4. Results

4.1 Carbonate vein abundance

Aragonite veins make up >90% of the carbonates recovered from both sites. Estimating the abundance of carbonate veins is of interest to assess the CO_2 uptake due to carbonate veining in exhumed mantle rock. The following estimates are based on detailed visual core logging conducted during Leg 209 (Shipboard Science Party, 2003). Holes 1271A and 1271B are within 90 m of each other. Hole 1271A was drilled to 44.8 mbsf (meters below seafloor) and recovered 12.9% of dunite cut by gabbroic dikes. 6.8 vol.% of the core are veins, of which 2.1% is aragonite, leading to an estimated aragonite content of 0.14 vol.%. Hole 1271B is 103.8 m deep, and 15.3% of basement were recovered. The core comprises pervasively serpentinized harzburgite and dunite with subordinate gabbroic and troctolitic rocks. 3.1 vol.% of the core are veins, of which 5.3% is aragonite (total aragonite content of 0.16 vol.%). Hole 1274A is 155.8 m deep and recovered 22.2% of core with 1.5% veins, of which 11.3% is aragonite. Late brittle deformation is indicated by non-cohesive fault gauge developed at a depth of 90 mbsf in Hole 1271B and 95 mbsf in Hole 1274A. No carbonate veins were observed in the 60 m of basement below the fault gauge in Hole 1274A, suggesting that veining may be restricted to the hanging wall of the fault.

4.2 Age dates and U-Th disequilibrium

Results of age dating are summarized in Table 1 with additional U-Th isotopic data provided in Table 2. The calcite veins from the detachment fault rocks at Site 1271 are all radiocarbon-dead, indicating formation more than 55.3 kyrs ago. Radiocarbon ages of aragonite veins from Hole 1274A range between 2 and 12 kyrs. Differences between the $^{14}C/^{12}C$ in surface and deep waters were not taken into account when

converting the radiocarbon age into a calendar age, and may add uncertainty on the order of few hundreds of years in the Holocene, and up to a thousand years during the last deglaciation (Keigwin 2004, Robinson et al., 2005).

The U concentrations of the U-Th dated aragonite veins range from 0.35 to 1.86 ppm with measured $^{234}U/^{238}U$ activity ratios (reported as ‰ deviation from secular equilibrium, $\delta^{234}U$) of 71 to 146 ‰ (Table 2). ^{232}Th concentrations range from 0.023 to 2.04 ppb. Raw ages for the samples are 122.9 ± 1.1 ka for the sample from Hole 1271B and 10.3 ± 0.05 ka and 8.5 ± 0.06 ka for the two samples from Hole 1274A. The accuracy of our calculated ages is affected by the presence of ^{230}Th that was incorporated into the carbonate at formation. This initial ^{230}Th is generally accounted for by using the measured ^{232}Th and an assumed initial $^{232}Th/^{230}Th$. Seawater data are sparse, but an Atlantic profile measured at ~8ºN gave dissolved $^{232}Th/^{230}Th$ ratios of ~3,000-8,000 at water depths greater than 1,000m (Moran et al., 2002). We use the average value of 5,858 to account for initial Th. The uncertainty on the correction is calculated using a range of $^{232}Th/^{230}Th$ values from the lowest measured dissolved water column value (3,000) and a typical detrital value (400,000; e.g., Henderson et al., 2001). The low ^{232}Th concentrations of two of the samples result in small age corrections. The sample from core 14 in Hole 1274A has a much higher ^{232}Th concentration, > 2 ppb, causing the age correction to dominate the uncertainty on the final age, 8.6 + 1.8 / -0.4 ka. A discussion of potential diagenetic alteration is given in section 5.2.

U-Th disequilibrium ages of the two samples at site 1274 correspond closely with the radiocarbon ages, and the dead radiocarbon ages at 1271 are consistent with our U-Th disequilibrium data. Both radiocarbon and U-Th disequilibrium ages for Site 1271 suggest that the aragonite veins are much younger than the hypothetical exposure ages of 700 kyrs (Site 1274) and 1500 kyrs (Site 1271) calculated from a half-spreading rate of 12 mm/yr and the distance between the drill site and the onlap of

the hanging wall. These young ages indicate fracturing and fluid circulation in the recent history, indicative of prolonged fluid-basement interaction during exhumation and uplift of lithospheric mantle in these settings.

U-Th disequilibrium dating of the calcite veins from Site 1271 was not possible due to the extremely low U concentrations (<100 ppb) of these samples (Table 1). Their age is hence uncertain.

4.3 Isotopic (O, C, Sr, Li) composition

Results of O-C-Sr-Li isotopic investigation are given in Table 1. Oxygen isotopic ratios range from 32.7 to 36.4‰ $\delta^{18}O_{SMOW}$ for aragonite veins (n = 22) and from 8.4 to 18.3‰ for calcite veins (n = 4). Calculated formation temperatures of the synkinematic calcite veins yield formation temperatures between 86 and 169°C. A $\delta^{18}O$ of the fluid of 0‰ was assumed in these calculations. The temperatures calculated for the calcite veins would be higher by 15 to 22°C if a fluid $\delta^{18}O$ composition of +2‰, corresponding to the most ^{18}O-enriched fluids from hydrothermal vents (Shanks, 2001), was assumed. The $\delta^{18}O$ data of the aragonites reveal that these veins formed at temperatures <14°C, with temperatures increasing downhole (Fig. 3). Four aragonite veins from Site 1271 yielded O-isotope temperatures slightly below 0°C, which is inconsistent with current seafloor temperatures in the 15°N area (2.5°C; Marbler et al., 2010). The high $\delta^{18}O_{SMOW}$ values >36‰, which lead to these exceptionally low temperatures, are not uncommon for peridotite-hosted carbonate veins (cf. Früh-Green et al., 2003; Eickmann et al., 2009). The most likely explanation is that these veins formed during a glacial maximum when the $\delta^{18}O_{SMOW}$ value of North Atlantic deep-sea water seawater was greater than the present-day value (0.22‰; Shanks, 2001).

□□□ $\delta^{13}C_{PDB}$-values of aragonite veins range between -2 and +3‰ typical of marine carbonates. Aragonite veins from Site 1271 are about 2‰ lighter (+0.3±1.0‰) in

$\delta^{13}C_{PDB}$ than those from Site 1274 (2.3±0.6‰). At both sites, t□□ $\delta^{13}C_{PDB}$ values appear to decrease somewhat with increasing subbasement depth. Three of the four calcite samples from Site 1271, reveal $\delta^{13}C_{PDB}$ compositions between +7.2 and +8.7‰, which is unusually heavy when compared with hydrothermal calcites veins from mantle rock in the Lost City and MARK areas ($\delta^{13}C_{PDB}$<+4.5‰; Alt and Shanks, 2003; Früh-Green et al. 2003).

$^{87}Sr/^{86}Sr$ compositions of most aragonite samples are between 0.70915 and 0.70917, virtually identical to the Sr isotope composition of modern seawater (0.70916; Banner, 2004). One sample (1274A 4R2 18-25cm) with a lower value of 0.70907 also has an anomalously high formation temperature of 11°C, suggesting that some exchange between basement fluid and rock took place. The Sr isotope compositions of the calcites range between 0.70387 and 0.70641. Three of the four calcite samples have unradiogenic values that are similar to those of 350-360°C hot vent fluids sampled in the Logatchev (0.7034; Amini et al., 2008) and Rainbow hydrothermal fields (0.7037-0.7041; Douville, 1999).

□□□δ^{7}Li-values for calcites range between +3.3 and +8.6‰, close to or slightly above the δ^{7}Li composition of the upper mantle (e.g., Elliott et al., 2004). Aragonite veins show δ^{7}Li compositions between +14.5 and +20.6‰, significantly lighter than seawater (~30‰; Hall et al., 2005; Pistiner and Henderson, 2003).

4.4 Chemical composition

The aragonite veins reveal the high Sr (5788-12328 ppm) and U (84-4926 ppb) contents expected for low-temperature seawater precipitates (Table 1). Subtle decreases in Sr/Ca and Mg/Ca are consistent with minor interactions with the basement as described previously by Coggon et al. (2004). Hydrothermal calcites/dolomites, however, are low in U (12-85 ppb), which is depleted from seawater during hydrothermal interaction with the basement (Michard et al., 1983;

Wheat and Mottl, 2000). The differences between the calcites and aragonites are most pronounced in their REE+Y patterns (Fig. 4). Data from calcite and calcite-dolomite veins resemble hydrothermal fluid patterns, characterized by light REE enrichment compared to seawater, positive Eu anomalies (Eu/Eu*= 9-617) and a positive Y anomaly (Y/Y*=Y/Sqrt(Dy*Ho)=8-17). Aragonites show seawater-like patterns with small negative Ce anomalies (Ce/Ce*=0.23-1.00), and pronounced positive Y anomalies (Y/Y*=7-201). Trace element abundances and ratios do not show systematic relations with basement depth.

There are two aragonite veins with REE pattern that deviate from those shown in Figure 4. Both have unusually high REE+Y concentrations. One of the samples (1274A 4R2 18-25 cm) also has unusually high U concentrations (8706 ppb) and the other one (1274A 1R1 8-15 cm) has the lowest U concentration measured (84 ppb). The sample with the high U concentrations may have been contaminated with Fe-oxyhydroxide. The aragonite with the low U concentrations probably precipitated from a fluid that had interacted with the basement more than the others. Both loss of U and gain in REE are expected consequences of fluid-rock interactions.

5. Discussion

Our observations and data suggest multiple stages of carbonate formation: (1) syntectonic calcite veins related to un-roofing along detachment faults and (2) aragonite veining during uplift and fracturing. These veins allow critical new insights into fluid flow and mass transfers during denudation and uplift of lithospheric mantle in the ocean basins.

5.1 Implications of calcite vein composition for fluid flow in faults

The unradiogenic $^{87}Sr/^{86}Sr$ values of most calcite veins resemble those of high-temperature (350-360°C) hydrothermal fluids from peridotite-hosted hydrothermal systems. In general, intense Sr exchange between fluid and basement is expected for high temperatures and low water-to-rock ratios, typical of the deepest and hottest parts of submarine hydrothermal circulation systems (James et al., 2003; Teagle et al., 1998). The same applies for the Li isotopic composition of the calcite veins, which are rock-dominated (+3.3 and +3.5‰ in the sample with the lowest $\delta^{18}O$ values). At temperatures around 350ºC, the fractionation factor between ^{6}Li and ^{7}Li is 0.996 (Chan and Edmond, 1988). Hence, fluids corresponding to the lowest $\delta^{7}Li$ value of our calcite samples are expected to have $\delta^{7}Li$ values of ~+7‰. This number is similar to the fairly uniform $\delta^{7}Li$ composition of hydrothermal vent fluids (Foustoukos et al., 2004). Hence, the Li and Sr isotopic composition of the calcite veins points to precipitation from a high-temperature hydrothermal fluid (350-400°C). This interpretation is corroborated by the $\delta^{13}C$ values of three (of four) calcite samples, which lie between +7.2 and +8.7‰. Such high $\delta^{13}C$ values suggest enrichment of ^{13}C through partial reduction of seawater carbonate to ^{12}C-rich methane (Alt and Shanks, 2003). The only reasonable explanation for the heavy $\delta^{13}C$ compositions is thermogenic methanogenesis, which requires temperatures in excess of 350°C (McCollom and Seewald, 2001).

While the Li and Sr isotope data correlate with each other, the C isotopes seem to be decoupled from these isotope systems. Sample 1271A 1R2 28-31 cm has low $\delta^{7}Li$ and $^{87}Sr/^{86}Sr$ values, but does not reveal the enrichment in ^{13}C displayed by the other samples. The data set is too small to attempt a meaningful assessment of the different behaviours. Generally, carbon isotopes are decoupled from tracers like Sr and Li isotopes, because CO_2 is added to the system via magmatic degassing, partly removed from the fluids upon carbonate precipitation, and partly reduced to methane by dihydrogen produced during serpentinization. These processes do not affect Sr

and Li, but they do affect C isotopes. Degassing may be episodic, and hydrogen production and CO_2 reduction are very much kinetically controlled. The variability in carbon isotope compositions of the calcite veins in the fault rocks likely reflects this complexity.

Although the Li-Sr-C isotopic evidence indicates precipitation of the calcites from fluids that had interacted with basement at temperatures of 350 to 400°C, the actual formation temperatures derived from O isotope thermometry are considerably lower (< 170°C for $\delta^{18}O_{fluid}$=0‰ and < 200°C for $\delta^{18}O_{fluid}$=2‰). When formation temperatures from O isotopes are plotted versus the Sr isotopic composition (Fig. 5), the data lie far below the line calculated for isenthalpic mixing of 360°C vent fluid and seawater. The combined isotopic data of the carbonate veins hence indicate that the hydrothermal fluids must have cooled considerably during slow upward migration along the fault. The detachment fault at Site 1271 was penetrated by deeply rooted fluids, which apparently did not use the fault as a conduit for rapid discharge to the seafloor. It has been suggested that detachment faults provide conduits, along which hydrothermal solutions can discharge and form black smoker type systems at the seafloor (McCaig et al., 2007). The detachment rocks from the metamorphic core complex at 15°45'N investigated by McCaig et al. (2007) are talc-rocks which are completely reset isotopically by a high flux of hydrothermal fluid. In contrast, rocks from Sites 1270 and 1271 (Fig. 1) are less deformed and show little evidence for metasomatism in the form of massive talc formation (Schroeder et al., 2007; Jöns et al., 2009). The calcite data presented here indicate that, while the precipitating fluids did have black-smoker-type characteristics, they were conductively cooled during slow ascent up the detachment fault. This result suggests that not all detachment faults are subjected to rapid fluid discharge and large fluxes of hydrothermal fluid.

5.2 Implications of aragonite vein composition for seawater-rock interactions and the geothermal gradient

The abundance of aragonite veins with uniform seawater-like signatures and similar ages throughout the uppermost basement, allows us to extract information on the thermal state of the uppermost crust using temperature-dependent oxygen isotope fractionation. This approach is best validated for aragonites from Hole 1274A, which are uniformly young (~8.5 kyrs) and minimize the effects of glacial-interglacial changes of deep-water $\delta^{18}O$ composition. To use the aragonites for reconstructing temperature of precipitation, we assume that circulating fluids and basement were thermally equilibrated and that the initial seawater-like oxygen isotope composition ($\delta^{18}O_{SMOW}$=0.22‰) is not changing as aragonite precipitates. The aragonite formation temperatures slightly increase down-hole from typical bottom water temperatures to ~14°C at about 85 mbsf (Fig. 3). One sample (1274A 4R-2 18-25 cm) deviates from the trend. This is the sample with the anomalously high U content and the only aragonite sample with $^{87}Sr/^{86}Sr$ rations significantly lower than that of modern seawater. The Sr isotope evidence suggests that the sample was precipitated from a seawater-derived fluid that had interacted with the basement. We discarded this anomalous sample in estimating the geothermal gradient. Generally, an influence of preferential uptake of ^{18}O during progressive fluid-rock interaction cannot be ruled out for any of the samples, but the effect this exchange would have on the fluid composition is likely very small (tenth of per mil in $\delta^{18}O$; Bowers and Taylor, 1985). Overall, the data suggest a decrease in $\delta^{18}O$ by 2 to 3 ‰ in the uppermost 80 m subbasement. Given that 1‰ in $\delta^{18}O$ corresponds to 4°C temperature change, we project a geothermal gradient of 100-150°C/km for the uppermost crust. This estimated gradient can be compared to a steady state conductive thermal gradient in the area, which can be derived from a thermobarometry-based assessment of lithospheric thickness. Both high-pressure

liquid lines of descent of Atlantic MORB and thermobarometry-based appraisal of olivine-plagioclase-two pyroxene-spinel cumulates from Site 1275 in the 15°45'N area suggest a conductive boundary layer thickness of 20-30 km (Shipboard Science Party, 2003; Kelemen et al., 2007). With an assumed temperature at the base of the lithosphere of 1300ºC a steady-state geothermal gradient of 40-70°/km can be estimated. The geothermal gradient derived from the down-hole distribution of $\delta^{18}O$ values of aragonites is considerably higher, indicating that the basement is not at a thermal steady state. The most likely explanation for the increased geothermal gradient is tectonic advection of heat related to high uplift rates (e.g., Cannat et al., 2004)

Strontium isotope ratios of aragonites are nearly uniform and very similar to modern seawater ($^{87}Sr/^{86}Sr$ ~0.70916). Based on these seawater-like $^{87}Sr/^{86}Sr$ ratios, we infer that neither Sr exchange between fluid and rock at low temperatures nor mixing with upwelling deeply rooted fluids took place, as both processes would significantly lower the $^{87}Sr/^{86}Sr$ ratio of the aragonites. Despite negligible chemical and Sr isotopic variability in aragonite compositions, δ^7Li values vary by 6‰. Based on Δ^7Li (δ^7Li_{Fluid} - $\delta^7Li_{Aragonite}$) between 8 and 12‰ at T=25ºC (Marriott et al., 2004; Gabitov et al., 2011) and a $\delta^7Li_{Seawater}$ of 30.8 (Rosner et al., 2007) one would expect seawater precipitates of aragonite to have a δ^7Li composition between +18 and +23‰. Most of the Li isotopic compositions of the Leg 209 aragonite veins (ranging between +14.5 and +20.6‰) fall within this expected range. The values < +18‰ could be related to low formation temperatures, e.g., if Δ^7Li was >12‰ at 2°C. The higher values (i.e. less fractionation relative to seawater) may be due to increasing temperature or may indicate progressive depletion of ^6Li compared to ^7Li as seawater penetrates the basement and water-rock interaction takes place. In interactions with seawater, both mafic and ultramafic basement preferentially picks up ^6Li (e.g., α@2°C=0.981; Chan

et al., 1992; Chan et al., 2002) and Li partitions into the solid phase at low temperatures (Seyfried et al., 1984; Chan et al., 2002; Vils et al., 2009). The resulting basement fluids will become depleted in Li and enriched in ^{7}Li, and therefore the isotopically heavy aragonites may have precipitated from such slightly evolved seawater-derived solutions. It appears that Li isotopes are much more sensitive to seawater-basement exchange at low temperatures than Sr isotopes. Another geochemical tracer known to respond quickly to seawater-rock interactions is REE+Y concentrations. Upon seawater-rock interactions, the much higher REE+Y contents of rocks are expected to superimpose a rock-like pattern to the fluids that may be modified by differential mobility of REEs due to differences in aqueous complex stability (e.g., Bau, 1991; Bach and Irber, 1998). The aragonites analyzed, however, show little indication of rock interaction, as the Y/Ho ratios are still seawater-like.

This conclusion is corroborated by the initial U isotope ratios ($\delta^{234}U_{initial}$) which can be back-calculated using the U-Th age, and used to screen marine carbonates for diagenetic overprints. This approach requires that the carbonate incorporates the same $\delta^{234}U$ value as seawater at formation (146 ‰), and that seawater has a known $\delta^{234}U$ history. A variety of biogenic and inorganic marine carbonates have been shown to incorporate seawater $\delta^{234}U$ and this value is not thought to have changed by more than one per cent over the last few hundred thousand years (Bard et al., 1991; Gallup et al., 1994; Henderson, 2002; Robinson et al., 2004). Our results show that $\delta^{234}U_{intial}$ data of both veins from Site 1274 are close to the seawater value. The $\delta^{234}U_{initial}$ of the sample from Site 1271 is lower than seawater at 99 ‰. There are two possible explanations for this anomaly: diagenetic perturbation of the U-series systematics, or a modified-seawater origin for the uranium. First we consider diagenesis. Loss of ^{234}U and ^{230}Th following an alpha-recoil model would give an age of 144 ka (Thompson et al., 2003), but would not explain the low uranium

concentration. Continuous uranium loss from 1.3 to 0.35ppm with no loss of thorium gives an age of ~36ka, but a low $\delta^{234}U_{initial}$ of 78 ‰. Alternatively the low U concentration and $\delta^{234}U_{initial}$ values may be original if the seawater was altered during its flow through the vein system before precipitation of this carbonate. In this case, the observed $\delta^{234}U_{initial}$ of 99 ‰ may reflect pristine carbonate. A combination of altered seawater origin and some diagnesis cannot be ruled out.

Overall, our data indicate very limited interaction between the ultramafic rocks and seawater during basement uplift at Sites 1271 and 1274. However, at both sites the downhole variations O isotope composition point to an increase in precipitation temperature with depth: Li isotope variations mirror this trend, suggesting that Li isotope exchange between fluid and basement may take place at low temperatures (<14°C).

5.3 Aragonite veining as sink of CO_2

Ages indicate episodic aragonite vein formation, some of it fairly recent (e.g., 2-12 kyrs at Site 1274). The overall aragonite vein abundance at both sites is ~0.2 vol.%, equivalent to an estimated CO_2 uptake of ~0.1 wt.%. This mass change is similar to what was proposed for uplifted gabbroic basement (Bach et al., 2001) and sedimented ridge flanks (Alt et al., 1996; Bach et al., 2004), but much smaller than the CO_2 uptake estimated for Cretaceous and Jurassic volcanic ridge flank crust (2-3 wt.% CO_2; Alt and Teagle, 1999; Staudigel et al., 1996). Unless the 80-85% of basement not cored has dramatically higher vein abundance, it appears that mantle rocks exposed at the seafloor take up less CO_2 than the equivalent volume of basaltic crust. This is likely due to the greater porosity of basaltic crust and to the ease with which basaltic glass weathers and releases Ca to the interacting seawater-derived solutions. Although the capacity of peridotite for sequestering CO_2 is great (Kelemen and Matter, 2008), our data suggest that low-temperature oxidative

alteration of exhumed mantle is probably not a globally important sink for CO_2. This conclusion is corroborated by the general scarcity of low-temperature aragonite veins in serpentinized mantle from other drill core (Site 895 in the Hess Deep; Blusztajn and Hart, 1996, and Site 920 south of the Kane Fracture Zone; Alt and Shanks, 1998). All these sites are in young lithosphere, however, and the estimates of CO_2 uptake may go up if fracturing and carbonate veining continues for tens of millions of years. This possibility can be examined only by drilling old rift mountains.

6. CONCLUSIONS

Carbonate veins in abyssal peridotite at 15°20'N encompass two distinct types formed under vastly different conditions. Calcite veins in detachment fault rocks at Site 1271 were generated from hydrothermal fluids similar in isotopic (Sr, C, Li) and geochemical (REE-Y) characteristics to 350°C hot vent fluid discharging in the nearby Logatchev black smoker field. However, formation temperatures ($\delta^{18}O$-thermometry) are significantly lower, indicating conductive cooling during slow ascent from deeper sources. This is in contrast to previously investigated detachment fault rocks that were subjected to high flux of hydrothermal fluids, indicating that not all of these major faults facilitate rapid upflow of hydrothermal fluids at all times.

The majority of radiocarbon ages of aragonite veins from Site 1274A clusters around 8.5 kyrs. This uniformly young aragonite formation is supported by two U-Th disequilibrium ages from Site 1274 of 8.6 and 9.0 kyrs, respectively. At Site 1271 aragonites formed earlier, and the age difference between aragonite formation at Sites 1271 and 1274 is reflected by more intense seafloor weathering in the vein halos at Site 1271.

The aragonite veins formed from fairly unmodified seawater in the hanging wall of fault gauge in depths of about 90 m below the seafloor. The scarcity of aragonite and

the limited depth extent assign a minor role to young abyssal peridotites as a sink for CO_2 in the oceanic ridge environment.

Systematically decreasing $\delta^{18}O$ values indicate increasing temperatures with depth. A downhole increase in $\delta^{7}Li$ values may also be indicative of increasing temperatures of precipitation (and less fractionation relative to seawater). Since age determinations show that the aragonite formed recently over a narrow time interval a geothermal gradient of 100-150°C/km for the uppermost crust can be estimated. This gradient is much steeper than the estimated conductive thermal gradient in the area (40 and 70ºC/km), which likely indicates that the lithosphere in this area of rapid uplift is not yet at thermal steady state.

ACKNOWLEDGMENTS

We thank T. Fujiwara for providing the detailed bathymetric data used in Fig. 1. This research used samples provided by the Ocean Drilling Program (ODP). ODP was sponsored by NSF and participating countries under the management of Joint Oceanographic Institutions. We thank two anonymous reviewers for helpful comments and suggestions. WB, MR, and NJ thank the Deutsche Forschungsgemeinschaft (grant no. BA1605/2) for funding. NJ acknowledges support from the DFG-Research Center/Excellence Cluster ‚The Ocean in the Earth System'

REFERENCES

Alt, J.C. et al., 1996. Ridge flank alteration of upper oceanic crust in the eastern Pacific: A synthesis of results for volcanic rocks of Holes 504B and 896A., in: Alt, J.C., Kinoshita, H., Stokking, L.B., Michael, P.J. (Eds.), Proc. ODP, Sci. Results. Ocean Drilling Program, College Station, TX, pp. 435-450.

Alt, J.C., Shanks, W.C., 1998. Sulfur in serpentinized oceanic peridotites: Serpentinization processes and microbial sulfate reduction. J. Geophys. Res. 103, 9917-9929.

Alt, J.C., Shanks, W.C., 2003. Serpentinization of abyssal peridotites from the MARK area, Mid-Atlantic Ridge, Sulfur geochemistry and reaction modeling. Geochim. Cosmochim. Acta 67, 641-653.

Alt, J.C., Teagle, D.A.H., 1999. The uptake of carbon during alteration of ocean crust. Geochim. Cosmochim. Acta 63, 1527-1535.

Alt, J.C., Teagle, D.A.H., 2003. Hydrothermal alteration of upper oceanic crust formed at a fast-spreading ridge: mineral, chemical, and isotopic evidence from ODP Site 801. Chem. Geol. 201, 191-211.

Amini, M. et al., 2008. Calcium isotope ($\delta^{44/40}$Ca) fractionation along hydrothermal pathways, Logatchev Field (Mid-Atlantic Ridge, 14°45'N). Geochim. Cosmochim. Acta 72, 4107-4122.

Bach, W. et al., 2001. The geochemical consequences of late-stage low-grade alteration of lower ocean crust at the SW Indian Ridge: Results from ODP Hole 735B (Leg 176). Geochim. Cosmochim. Acta 65, 3267-3287.

Bach, W. et al., 2004. Variable seawater-peridotite interactions – First insights from ODP Leg 209, MAR 15ºN. Geochemistry, Geophysics, Geosystems 5: Q09F26, doi: 10.1029/2004GC000744.

Bach, W., Irber, W., 1998. REE mobility in the oceanic lower sheeted dyke complex: Evidence from geochemical data and leaching experiments. Chem. Geol. 151, 309-326.

Banner, J.L., 2004. Radiogenic isotopes: systematics and applications to earth surface processes and chemical stratigraphy. Earth-Sci. Rev. 65, 141-194.

Bard, E. et al., 1991. Uranium-234 anomalies in corals older than 150 000 years. Geochimica et Cosmochimica Acta 55, 2385-2390.

1 Bau, M., 1991. Rare-earth element mobility during hydrothermal and metamorphic
2 fluid-rock interaction and the significance of the oxidation state of europium.
3 Chem. Geol. 93, 219-230.
4 Blusztajn, J., Hart, S.R., 1996. Sr and O isotopic ratios of aragonite veins from Site
5 895. In: C. Mevel, K.M. Gillis, J.F. Allan, P.S. Meyer (Editors), Proc. ODP Sci.
6 Results 147. Ocean Drilling program, College Station, 311-313.
7 Bonatti, E. et al., 1980. Aragonite from deep sea ultramafic rocks. Geochim.
8 Cosmochim. Acta 44, 1207-1215.
9 Bowers, T.S., Taylor, H.P., Jr., 1985. An intergrated chemical and stable-isotope
10 model of the origin of midocean ridge hot spring systems. J. Geophys. Res.
11 90, 12,583-512,606.
12 Cannat, M., Cann, J., Maclennan, J., 2004. Some hard rock constraints on the supply
13 of heat to mid-ocean ridges. In: C.R. German, J. Lin, L.M. Parson (Editors),
14 Mid-ocean ridges: hydrothermal interactions between the lithosphere and the
15 oceans. AGU Monograph Series 148, 111-149
16 Cannat, M., Fountaine, F., Escartin, J., 2010. Serpentinization and associated
17 hydrogen and mathane fluxes at slow-spreading ridges In: P. Rona, C.
18 Devey, J. Dyment, B.J. Murton (Editors), Diversity of Hydrothermal Systems
19 on Slow Spreading Ocean Ridges. AGU Monograph Series 188, 241-264.
20 Chan, L.H., Alt, J.C., Teagle, D.A.H., 2002. Lithium and lithium isotope profiles
21 through the upper oceanic crust: a study of seawater-basalt exchange at
22 ODP Sites 504B and 896A. Earth Planet. Sci. Lett. 201, 187-201.
23 Chan, L.H., Edmond, J.M., 1988. Variation of lithium isotope composition in the
24 marine environment: A preliminary report. Geochim. Cosmochim. Acta 52,
25 1711-1717.
26 Chan, L.H. et al., 1992. Lithium isotopic composition of submarine basalts:
27 implications for the lithium cycle in the oceans. Earth Planet. Sci. Lett. 108,
28 151-160.

Coggon, R.M. et al., 2004. Linking basement carbonate vein compositions to porewater geochemistry across the eastern flank of the Juan de fuca Ridge, ODP Leg 168. Earth Planet. Sci Lett. 219, 111-128.

Douville, E., 1999. Les fluides hydrothermaux oceaniques comportement geochimique des elements traces et des terres rares. Processus associes et modelisation thermodynamique. Ph.D. Thesis Thesis, University of Brest, France, Brest.

Edwards, R.L., Chen, J.H., and Wasserburg, G.J., 1986. ^{238}U-^{234}U-^{230}Th-^{232}Th systematics and the precise measurement of time over the past 500 000 years. Earth Planet. Sci. Lett. 81, 175-192.

Eickmann, B., Bach, W., Peckmann, J., 2009. Geochemical constraints on the modes of carbonate precipitation in peridotites from the Logatchev Hydrothermal Vent Field and Gakkel Ridge. Chemical Geology 268, 97-106.

Elliott, T., Jeffcoate, A., Bouman, C., 2004. The terrestrial Li isotope cycle: light-weight constraints on mantle convection. Earth Planet. Sci. Lett. 220, 231-245.

Escartín, J., Cannat, M., 1999. Ultramafic exposures and the gravity signature of the lithosphere near the Fifteen-Twenty Fracture Zone (Mid-Atlantic Ridge, 14°-16.5°N). Earth Planet. Sci. Lett. 171, 411-424.

Flesch, G.D., Anderson, A.R., Svec, H.J., 1973. A secondary isotopic standard for $^{6}Li/^{7}Li$ determination. Int. J. Mass Spectrom. Ion Phys. 12, 265-272.

Foustoukos, D.I. et al., 2004. Lithium isotopic systematics of hydrothermal vent fluids at the Main Endeavour Field, Northern Juan de Fuca Ridge. Chem. Geol. 212, 17-26.

Früh-Green, G.L. et al., 2003. 30,000 years of hydrothermal activity at the Lost City vent field. Science 301, 495-498.

1 Fujiwara, T. et al., 2003. Crustal evolution of the Mid-Atlantic Ridge near the Fifteen-
2 Twenty Fracture Zone in the last 5 Ma. Geochem. Geophys. Geosys. 4,
3 doi:10.1029/2002GC000364.
4 Gallup, C.D., Edwards, R.L., Johnson, R.G., 1994. The timing of high sea levels over
5 the past 200 000 years. Science 263, 796-800.
6 Hall, J.M. et al., 2005. Determination of the lithium isotopic composition of planktic
7 foraminifera and its application as a paleo-seawater proxy. Mar. Geol. 217,
8 255-265.
9 Henderson, G. M., 2002. Seawater ($^{234}U/^{238}U$) during the last 800 thousand years.
10 Earth and Planetary Science Letters 199, 97-110.
11 Jackson, M.G., Hart, S.R., 2006. Strontium isotopes in melt inclusions from Samoan
12 basalts: Implications for heterogeneity in the Samoan plume. Earth Planet.
13 Sci. Lett. 245, 260-277.
14 James, R.H., Allen, D.E., Seyfried, W.E.J., 2003. An experimental study of alteration
15 of oceanic crust and terrigenous sediments at moderate temperatures (51 to
16 350°C): Insights as to chemical processes in near-shore ridge-flank
17 hydrothermal systems. Geochim. Cosmochim. Acta 67, 681-691.
18 Jöns, N., Bach, W., Schroeder, T., 2009. Formation and alteration of plagiogranites
19 in an ultramafic-hosted detachment fault at the Mid-Atlantic Ridge (ODP Leg
20 209). Contrib. Mineral. Petrol. 157, 625-639.
21 Karlen, I. et al., 1968. Absolute determination of the activity of two ^{14}C dating
22 standards. Arkiv Geofysik 4, 465-471.
23 Kelemen, P.B., Kikawa, E., Miller, D.J. and Shipboard Science Party, 2007. Leg 209
24 summary: processes in a 20-km-thick conductive boundary layer beneath the
25 Mid-Atlantic Ridge, 14°–16°N. In: P.B. Kelemen, E. Kikawa, D.J., Miller
26 (Editors), Proc. ODP, Sci. Results. Ocean Drilling Program, College Station,
27 TX, pp. 1-33.

Kelemen, P.B., Matter, J., 2008. In situ carbonation of peridotite for CO_2 storage. Proc. Natl. Acad. Sci. U.S.A. 105, 17295– 17300.

Kim, S.-T., O'Neil, J.R., 1997. Equilibrium and nonequilibrium oxygen isotope effects in synthetic carbonates. Geochim. Cosmochim. Acta 61, 3461-3475.

Kim, S.-T., O'Neil, J.R., Hillaire-Marcel, C., Mucci, A., 2007. Oxygen isotope fractionation between synthetic aragonite and water: Influence of temperature and Mg^{2+} concentration. Geochim. Cosmochim. Acta 71, 4704-4715.

Marbler, H. et al., 2010. Geochemical and physical structure of the hydrothermal plume at the ultramafic-hosted Logatchev hydrothermal field at 14°45′N on the Mid-Atlantic Ridge. Mar. Geol. 271, 187-197.

Marriott, C.S. et al., 2004. Temperature dependence of δ^7Li, δ^{44}Ca, and Li/Ca during growth of calcium carbonate. Earth Planet. Sci. Lett. 222, 615-624.

McCaig, A.M., et al., 2007. Oceanic detachment faults focus very large volumes of black smoker fluids. Geology 35, 935-938.

McCollom, T.M., Seewald, J.S., 2001. A reassessment of the potential for reduction of dissolved CO_2 to hydrocarbons during serpentinization of olivine. Geochim. Cosmochim. Acta 65, 3769-3778.

Michard, A. et al., 1983. Rare-earth elements and uranium in high-temperature solutions from East Pacific Rise hydrothermal vent field (13°N). Nature 303, 795-797.

Moran, S.B. et al., 2002. Dissolved and particulate ^{231}Pa and ^{230}Th in the Atlantic Ocean: constraints on intermediate/deep water age, boundary scavenging, and ^{231}Pa/^{230}Th fractionation. Earth and Planetary Science Letters 203, 999-1014.

Pistiner, J.S., Henderson, G.M., 2003. Lithium-isotope fractionation during continental weathering processes. Earth Planet. Sci. Lett. 214, 327-339.

Reimer, P.J. et al., 2010, IntCal04 terrestrial radiocarbon age calibration, 0-26 cal kyr BP. Radiocarbon 46, 1029-1058.

Robinson, L.F., et al., 2004. Climatic control of riverine and Seawater uranium-isotope ratios. Science 305, 851-854.

Robinson, L.F. et al., 2005. Radiocarbon variability in the Western North Atlantic during the last deglaciation. Science 310, 1469-1473.

Rosner, M. et al., 2007. A Simplified, Accurate and Fast Method for Lithium Isotope Analysis of Rocks and Fluids, and δ^7Li Values of Seawater and Rock Reference Materials J. Geostandards Geoanal. Res. 31, 77-88.

Schroeder, T. et al., 2007. Nonvolcanic seafloor spreading and corner-flow rotation accommodated by extensional faulting at 15°N on the Mid- Atlantic Ridge, A structural synthesis of ODP Leg 209. Geochem. Geophys. Geosys. 8, Q06015, doi:10.1029/2006GC001567.

Seyfried, W.E., Jr., Janecky, D.R., Mottl, M.J., 1984. Alteration of the oceanic crust: implications for geochemical cycles of lithium and boron. Geochim. Cosmochim. Acta, 48 557-569.

Shanks, W.C. III, 2001. Stable isotopes in seafloor hydrothermal systems. In: J.W. Valley, D. Cole (Editors), Stable Isotope Geochemistry. Mineralogical Sociey of America, pp. 469-525.

Shipboard Science Party, 2003. Leg 209 Preliminary Report. ODP Prelim. Rpt., 209 [Online], Available from World Wide Web: <http://www-odp.tamu.edu/publications/prelim/209_prel/209PREL.PDF>. [Cited YYYY-MM-DD].

Staudigel, H. et al., 1996. Geochemical fluxes during seafloor alteration of the basaltic upper oceanic crust: DSDP Sites 417 and 418. In: G.E. Bebout, D.W. Scholl, S.H. Kirby, J.P. Platt (Editors), Subduction top to bottom. American Geophysical Union, Washington, D.C., pp. 19-38.

Sun, S.-s., McDonough, W.F., 1989. Chemical and isotopic systematics of oceanic basalts: implications for mantle composition and processes. In: A.D.

Saunders, M.J. Norry (Editors), Magmatism in the Ocean Basins. Geol. Soc. Spec. Pub., Oxford, pp. 313-345.

Teagle, D.A.H., Alt, J.C., Halliday, A.N., 1998. Tracing the chemical evolution of fluids during hydrothermal recharge: Constraints from anhydrite recovered in ODP Hole 504B. Earth Planet. Sci. Lett. 155, 167-182.

Thompson, W.G. et al., 2003. An open-system model for U-series age determinations of fossil corals. Earth Planet. Sci. Lett. 210, 365-381.

Vils, F., Tonarini, S., Kalt, A., Seitz, H.-M., 2009. Boron, lithium and strontium isotopes as tracers of seawater- serpentinite interaction at Mid-Atlantic ridge, ODP Leg 209. Earth Planet. Sci. Lett. 286, 414-425.

Wheat, C.G., Mottl, M.J., 2000. Composition of pore and spring waters from baby bare: Global implications of geochemical fluxes from a ridge flank hydrothermal system. Geochim. Cosmochim. Acta 64, 629-642.

Figure captions

Figure 1: Map of the 15°20'N Fracture Zone (data from Fujiwara et al., 2003) showing the locations of the study sites (1271 and 1274) and other ODP Leg 209 drill sites. Also displayed are photographs of aragonite and calcite veins as well as a sketch of carbonate vein distribution in the basement.

Figure 2: (a) Thin section scan (cros- polarized light) of calcite vein in sample 1271B 7R1 64-68 cm. (b) Thin section scan (cross-polarized light) of an aragonite vein with oxidation halo in sample 1271B 4R1 28-32 cm (B). (c) Thin section photomicrograph of calcite vein in sample 1271B 7R1 64-68 cm (plane-polarized light). (d) Cathodoluminescence photomicrograph, same field of view as in [c]. (e) Thin section photomicrograph of aragonite vein in sample 1271B 1R1 8-15 cm (plane-polarized light). (f) Cathodoluminescence photomicrograph, same field of view as in [e].

Figure 3: Isotopic compositions of aragonite veins from Holes 1271B and 1274A plotted versus depth below seafloor.

Figure 4: Selected REE+Y pattern of veins of calcite (filled symbols) and aragonite (open symbols). Calcite samples are from Hole 1271A, aragonites (sample name in italics) are from Hole 1271B (8R1, 62-64 cm) and 1274A (both from core 15). Chondrite values used for normalization are from Sun and McDonough (1989).

Figure 5: Plot of formation temperature (from oxygen isotopes) and Sr isotopic composition of carbonate veins. The Logatchev vent fluid (Amini et al., 2008) and an isenthalpic mixing trend between vent fluid and seawater are also shown. The calcite veins (filled symbols) indicate massive amounts of conductive cooling indicative of

very slow upflow rates. The aragonite veins (open symbols) have Sr isotope compositions similar to modern seawater.

***Research Highlights**

- First time carbonate abundance was estimated in ultramafic-type ocean lithosphere. Carbonate abundance is very low, indicating that CO2 is not sequestered in significant amounts during circulation of seawater through serpentinized basement.
- First time aragonite veins from ocean crust away from an active hydrothermal vent were age dated. The age dates are surprisingly young , indicating that veining occured in the latest stages of uplift. The veins allow the reconstruction of a sub-recent geotherm, by emplyoing O isotope thermometry.
- First time syn-kinematic calcite veins were analyzed. The data provide novel insights into fluid evolution in detachment faults. Sr, Li, and C isotopes clearly indicate temperatures >350°C in the root zone oft he fluids. However, O isotopes indicate much lower 90-160°C temperatures of precipitation. Unlike metasomatosed rocks from other locations (e.g., at 30°N on the Mid-Atlantic Ridge), the calcites record a regime of significant conductive cooling, hence very slow uprise of fluids. This shows that detachment faults may not always provide conduits for rapidly uprising hydrothermal solutions.

Figure1

Click here to download Figure: figure1.pdf

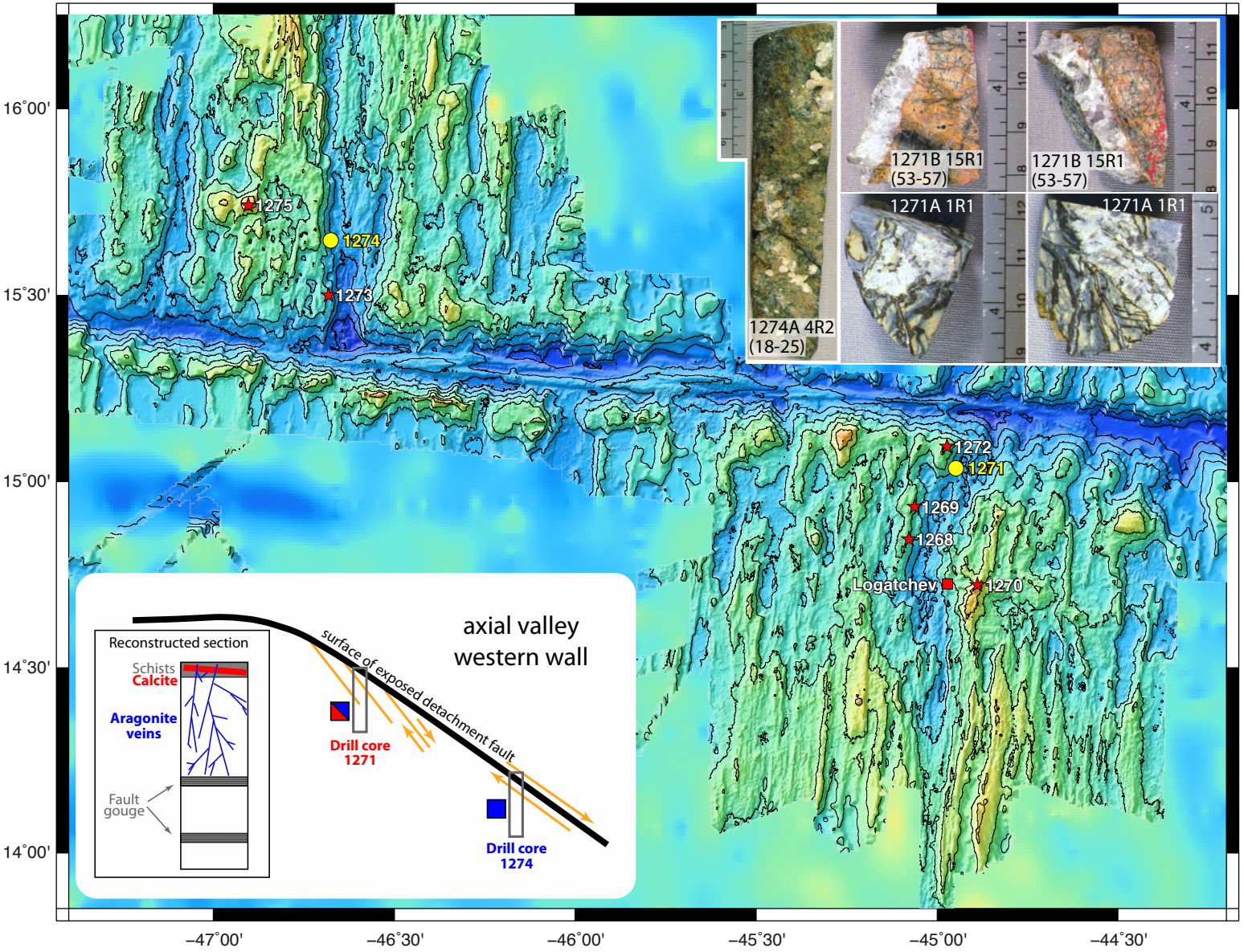

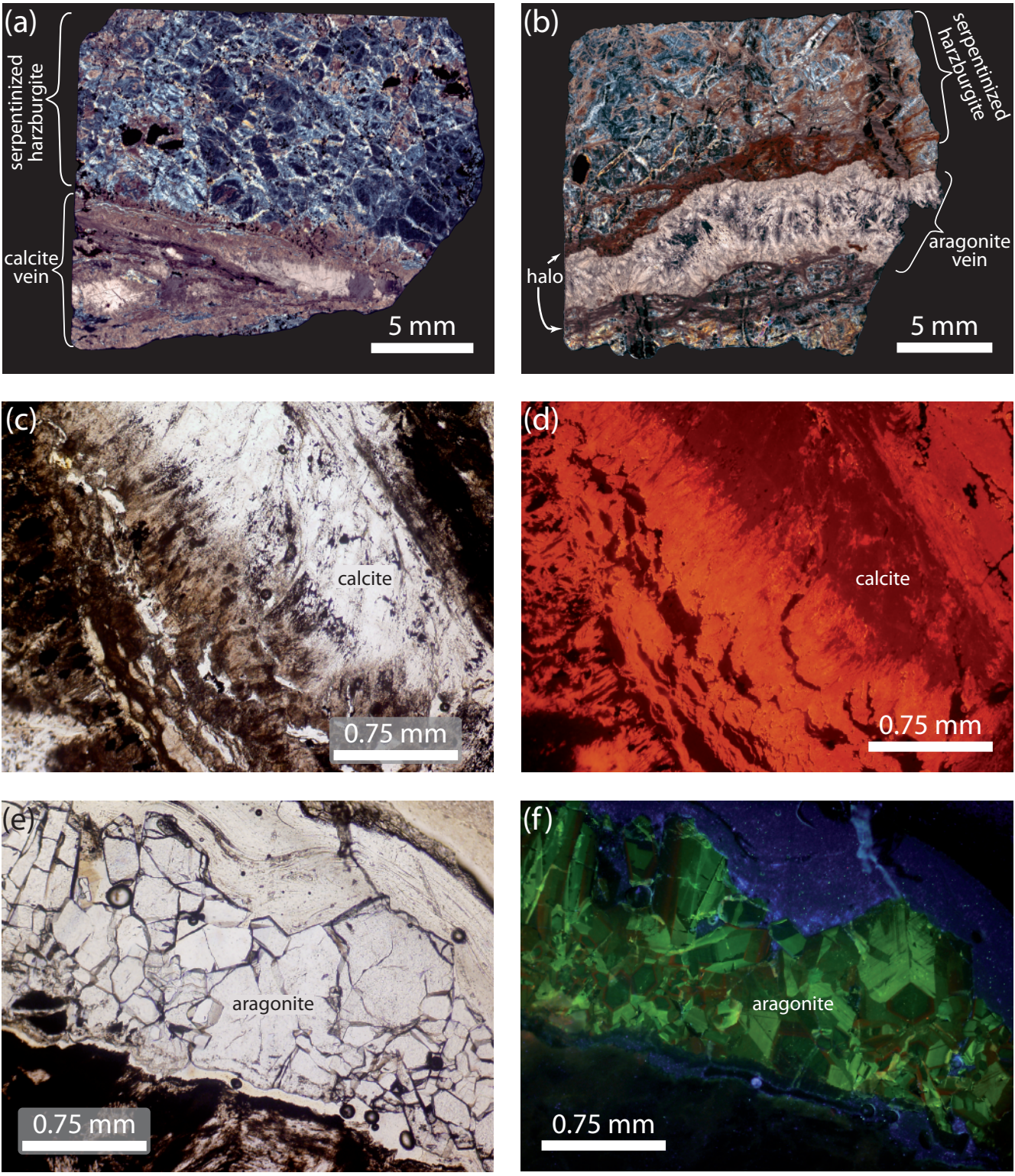
(a)
serpentinized harzburgite
calcite vein
5 mm
(b)
serpentinized harzburgite
aragonite vein
halo
5 mm
(c)
calcite
0.75 mm
(d)
calcite
0.75 mm
(e)
aragonite
0.75 mm
(f)
aragonite
0.75 mm

Figure3

Click here to download Figure: Figure3new.pdf

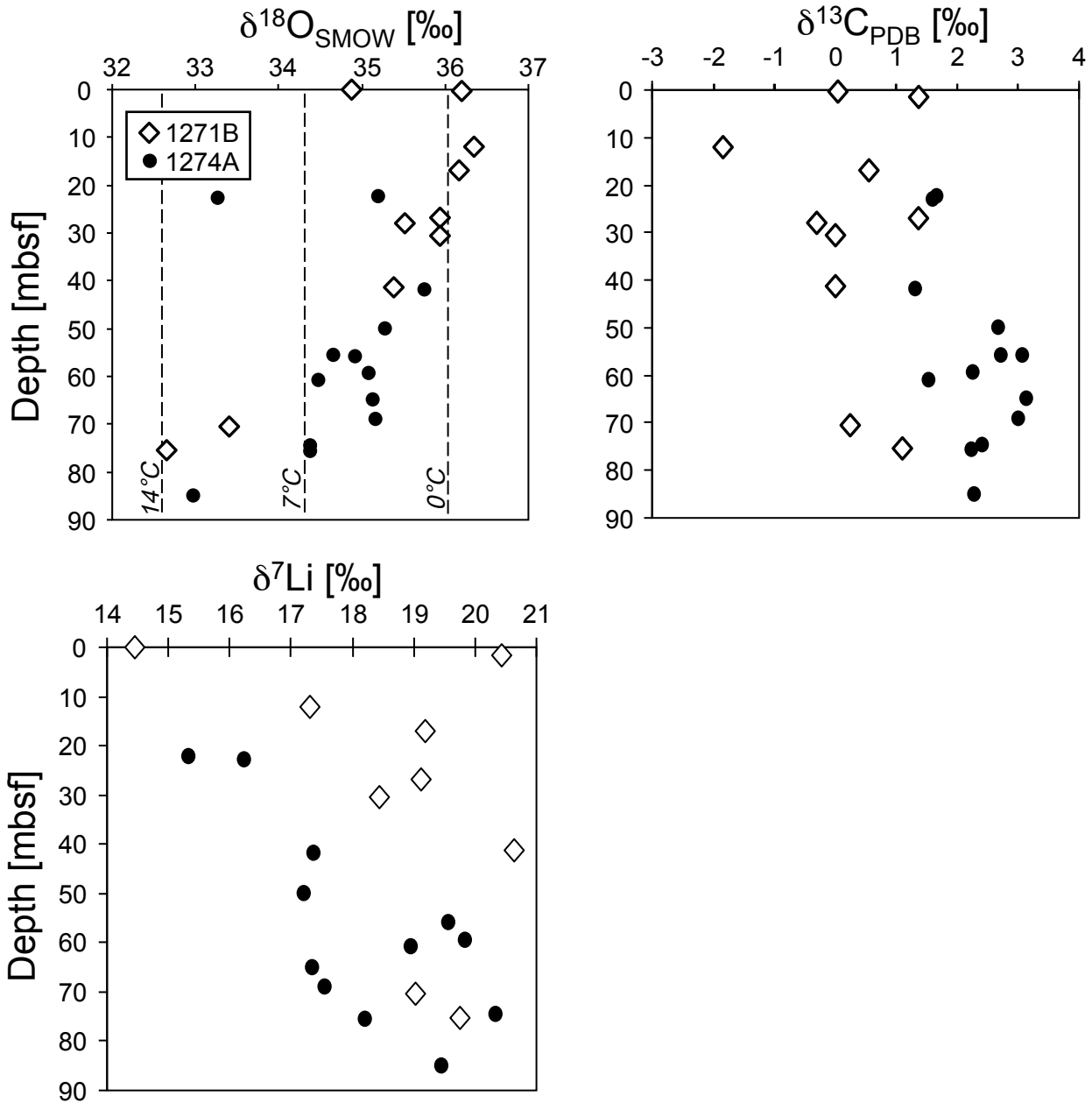

Figure4
Click here to download Figure: Figure4.pdf

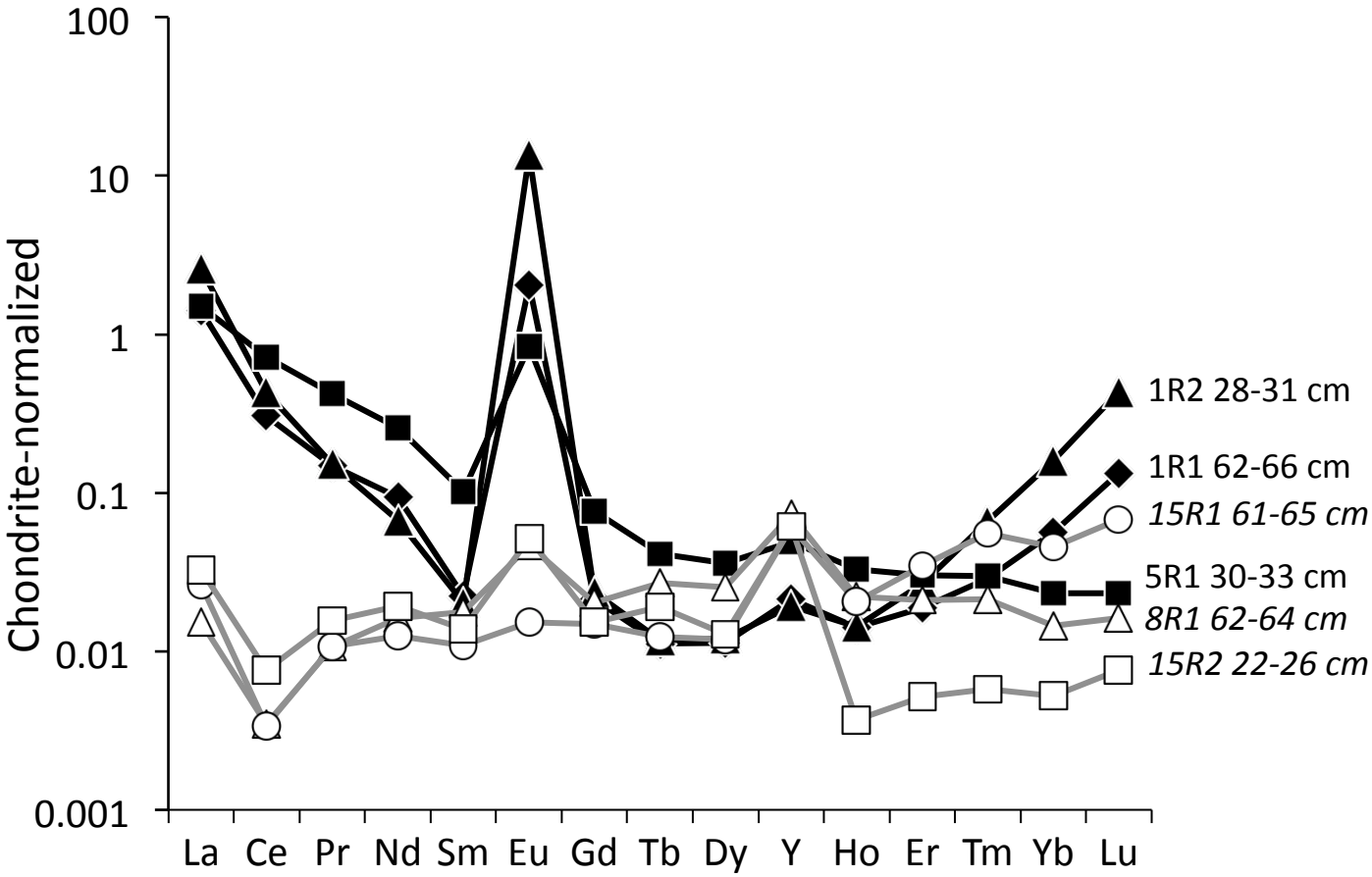

Figure5
Click here to download Figure: Figure5.pdf

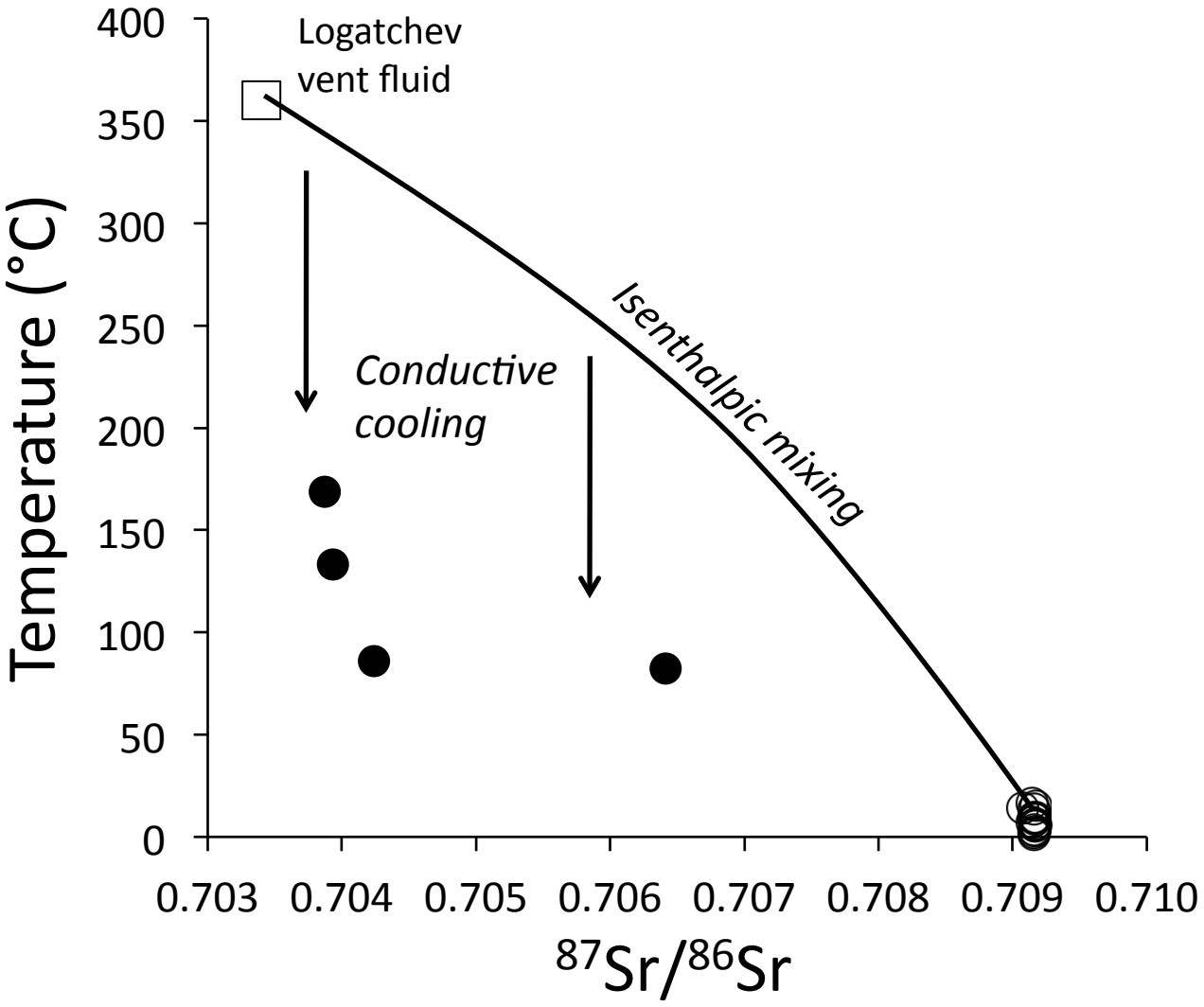

Table1

Click here to download Table: Table1_revised.xls

Table 1: Isotopic compositions and radiocarbon ages of carbonate veins

Sample	Depth (mbsf)	Minerals	$^{87}Sr/^{86}Sr$	^{7}Li	^{13}C PDB	^{18}O SMOW	^{18}O PDB	T (°C)	^{14}C age yrs
1271A 1R2 25-28 cm	1.7	Aragonite	0.709153	20.44	0.2	36.2	5.1	-1.6	
1271A 4R2 72-75 cm	30.5	Aragonite	0.709166	18.45	-0.3	34.7	3.7	4.5	>54900
1271B 1R1 8-15 cm	0.1	Aragonite	0.709146	14.45	1.4	34.9	3.9	3.9	>54900
1271B 2R1 5-11 cm	12.1	Aragonite	0.709160	17.30	-1.8	36.4	5.3	-2.2	
1271B 3R1 0-6 cm	17.0	Aragonite	0.709156	19.18	0.6	36.2	5.1	-1.5	
1271B 4R1 28-32 cm	26.9	Aragonite	0.709164	19.11	1.4	35.9	4.9	-0.5	>54900
1271B 8R1 62-64 cm	41.3	Aragonite	0.709163	20.63	0.0	35.4	4.3	1.8	
1271B 14R1 58-62 cm	70.4	Aragonite	0.709156	19.04	0.3	33.4	2.4	10.1	>54900
1271B 15R1 53-57 cm	75.3	Aragonite	0.709145	19.75	1.1	32.7	1.7	13.3	>54900
1274A 4R1 104-110 c	22.3	Aragonite	0.709169	15.34	1.7	35.2	4.2	2.6	2110
1274A 4R2 18-25 cm	22.9	Aragonite	0.709069	16.25	1.6	33.3	2.3	10.8	12000
1274A 8R2 40-44 cm	41.9	Aragonite	0.709159	17.37	1.3	35.8	4.7	0.3	8350
1274A 10R1 21-27 cm	50.1	Aragonite	0.709168	17.21	2.7	35.3	4.3	2.1	7050
1274A 11R1 84-88 cm	55.8	Aragonite	0.709167		3.1	34.7	3.6	4.8	
1274A 11R1 100-108	56.0	Aragonite		19.58	2.7	34.9	3.9	3.7	
1274A 12R1 6-14 cm	59.5	Aragonite	0.709166	19.85	2.3	35.1	4.1	3.1	6570
1274A 12R2 9-13 cm	61.0	Aragonite	0.709155	18.96	1.5	34.5	3.5	5.6	10450
1274A 13R1 61-66 cm	65.0	Aragonite	0.709167	17.35	3.2	35.1	4.1	2.9	8160
1274A 14R1 14-20 cm	69.1	Aragonite	0.709174	17.57	3.0	35.2	4.1	2.7	8730
1274A 15R1 61-65 cm	74.6	Aragonite	0.709160	20.35	2.4	34.4	3.4	6.0	10000
1274A 15R2 22-26 cm	75.7	Aragonite	0.709171	18.22	2.3	34.4	3.4	6.0	
1274A 16R1 129-134	85.0	Aragonite	0.709170	19.47	2.3	33.0	2.0	11.9	10100
1271A 1R1 62-66 cm	0.6	Calcite	0.704239	8.57	7.2	17.8	-12.7	86	
1271A 5R1 30-33 cm	38.4	Calcite	0.703872	3.29	7.9	8.4	-21.8	169	
1271A 1R2 28-31 cm	1.8	Cal/dolo	0.703933	3.51	0.2	12.0	-18.3	133	
1271B 7R1 64-68 cm	36.8	Cal/dolo	0.706413		8.7	18.3	-13.7	82	

Table2

Click here to download Table: Table2_U-Th.pdf

Table 2: Results of U-Th disequilibrium studies

Sample	^{238}U ppm	^{232}Th ppb	($^{232}Th/^{230}Th$) atom	$\delta^{234}U_{meas}$ ‰	($^{230}Th/^{238}U$) activity	raw age years	corrected age years	$\delta^{234}U_{initial}$ ‰
1271B 15R1 53-57 cm	0.3510 ± 0.0001	0.023 ± 0.004	5.4 ± 1.0	70.7 ± 2.1	0.7305 ± 0.0031	122893 ± 1118	122818 + 1219 - 1138	99.5 ± 1.3
1274A 14R1 14-20 cm	1.3005 ± 0.0004	2.035 ± 0.013	916.3 ± 4.8	143.2 ± 2.0	0.1034 ± 0.0005	10339 ± 53	8611 + 1770 - 391	146.3 ± 0.6
1274A 8R2 40-44 cm	1.8642 ± 0.0007	0.116 ± 0.012	44.1 ± 4.7	146.4 ± 2.1	0.0858 ± 0.0005	8480 ± 60	8412 + 135 - 76	149.6 ± 0.7

Table3

Click here to download Table: Table3_traces.pdf

Table 3: Trace element compositions of carbonate veins

Sample	Depth (mbsf)	Minerals	Sr ppm	Mg ppm	Na ppm	Li ppb	U ppb	Rb ppb	Cs ppb	La ppb	Ce ppb	Pr ppb	Nd ppb	Sm ppb	Eu ppb	Gd ppb	Tb ppb	Dy ppb	Ho ppb	Er ppb	Tm ppb	Yb ppb	Lu ppb	Y ppb	Pb ppb	Ba ppb
1271A 4R2 72-75 cm	30.5	Aragonite	8787	550	590	206	307	15	0.3	10	11	1.1	4.8	0.9	1.2	1.7	0.2	1.0	0.2	0.8	0.2	1.2	0.3	25	90	33
1271B 1R1 8-15 cm	0.1	Aragonite	9025	198	676	271	84	8.2	0.4	1816	4539	766	3441	610	84	663	67	335	55	98	8.0	26	2.6	1205	66	34
1271B 2R1 5-11 cm	12.1	Aragonite	9794	163	1308	320	4926	5.7	0.2	8.7	2.6	0.9	3.6	1.2	1.4	2.2	0.2	0.8	0.2	1.0	0.1	0.4	0.1	29	61	60
1271B 3R1 0-6 cm	17.0	Aragonite	10754	211	1283	570	1679	7.9	0.1	2.4	1.6	0.4	2.6	1.1	4.1	1.7	0.5	2.2	0.1	0.3	0.1	0.2	0.1	95	17	82
1271B 4R1 28-32 cm	26.9	Aragonite	11770	24	983	419	1721	4.3	0.1	0.8	1.2	0.1	1.0	0.3	0.3	0.8	0.2	0.4	0.0	0.7	0.2	1.3	0.4	33	1910	70
1271B 8R1 62-64 cm	41.3	Aragonite	9777	267	641	360	446	12	0.6	3.6	2.1	1.0	7.4	2.7	3	4.1	1.0	6.5	1.2	3.5	0.5	2.5	0.4	114	29	60
1271B 14R1 58-62 cm	70.4	Aragonite	9770	14	1240	261	1477	5.2	0.2	4.2	3.7	0.4	1.7	0.5	0.4	1.5	0.2	1.7	0.4	1.9	0.3	1.9	0.4	58	32	40
1271B 15R1 53-57 cm	75.3	Aragonite	5788	4.1	1053	92	265	2.9	0.1	58	41	4.4	20	1.8	0.3	2.3	0.2	0.7	0.3	1.3	0.3	1.6	0.4	34	22	23
1274A 4R1 104-110 cm	22.3	Aragonite	11374	1181	1296	475	2452	12	0.5	2.8	3.0	0.4	1.6	0.5	0.3	1.5	0.3	1.1	0.4	2.8	0.3	2.7	0.6	32	235	4.3
1274A 4R2 18-25 cm	22.9	Aragonite	10214	139	1421	609	8706	6.1	0.2	104	60	25	136	29	15	42	6.5	48	13	41	6.8	42	7.2	555	53	160
1274A 8R2 40-44 cm	41.9	Aragonite	10887	68	1388	417	3012	7.9	0.2	1.1	1.6	0.2	0.9	0.5	0.2	1.1	0.2	0.3	0.1	0.6	0.1	0.5	0.1	24	36	43
1274A 10R1 21-27 cm	50.1	Aragonite	11383	182	937	323	1881	6.5	0.7	1.8	2.9	0.4	0.1	0.3	0.3	1.7	0.3	2.2	0.9	5.3	1.2	8.3	1.7	54	106	40
1274A 11R1 84-88 cm	55.8	Aragonite	11048	210	1025	537	1454	7.1	0.1	1.4	0.9	0.1	2.1	1.0	4.0	1.8	0.5	2.6	0.2	0.9	0.2	1.7	0.4	99	18	90
1274A 11R1 100-108 cm	56.0	Aragonite	10880	160	970	493	1723	7.5	0.1	1.3	1.4	0.2	2.0	1.2	2.6	2.1	0.5	2.9	0.2	1.0	0.3	2.0	0.5	102	27	56
1274A 12R1 6-14 cm	59.5	Aragonite	11752	73	1028	348	2533	13	0.3	35	52	5	12	5.9	2.6	4.0	0.8	7.3	1.6	7.3	1.4	9.1	2.1	105	136	71
1274A 12R2 9-13 cm	61.0	Aragonite	10808	232	1177	380	1901	4.7	0.2	4.0	2.4	0.4	2.1	0.6	0.3	1.6	0.3	0.5	0.1	1.7	0.2	1.8	0.3	26	54	65
1274A 13R1 61-66 cm	65.0	Aragonite	11198	36	1145	370	1942	7.9	0.2	0.9	1.2	0.2	1.1	0.3	0.2	1.1	0.3	1.0	0.6	4.8	1.6	14.4	3.8	68	55	38
1274A 14R1 14-20 cm	69.1	Aragonite	12328	43	1192	563	2659	19	7.4	4.8	8.7	1.0	4.6	1.4	0.4	2.4	0.5	1.5	0.4	2.0	0.4	2.5	0.6	46	31	56
1274A 15R1 61-65 cm	74.6	Aragonite	10854	25	1128	393	1075	4.9	0.1	6.2	2.1	1.0	5.7	1.7	0.9	3.1	0.5	3.0	1.2	5.8	1.4	7.7	1.7	95	53	55
1274A 15R2 22-26 cm	75.7	Aragonite	10659	404	1248	549	2504	16	0.6	7.8	4.6	1.5	8.9	2.1	3.0	3.1	0.7	3.3	0.2	0.9	0.1	0.9	0.2	96	28	54
1274A 16R1 129-134 cm	85.0	Aragonite	9145	92	1202	281	2578	4.9	0.2	2.1	1.4	0.3	2.3	1.1	0.9	3.0	0.4	2.0	0.6	2.0	0.4	1.6	0.2	44	79	29
1271A 1R1 62-66 cm	0.6	Calcite	101	1206	105	133	33	16	0.5	335	186	14	43	3.4	119	4.4	0.4	2.9	0.8	3.1	0.7	10	3.4	33	60	25
1271A 5R1 30-33 cm	38.4	Calcite	64	44	15	104	12	5.0	0.3	353	439	40	118	16	48	16	1.5	9.2	1.9	5.0	0.8	3.9	0.6	77	38	2.3
1271A 1R2 28-31 cm	1.8	Cal/dolo	125	10184	68	456	31	12	0.5	612	264	15	31	3.1	785	4.9	0.4	3.0	0.8	4.4	1.7	27	11	30	51	13
1271B 7R1 64-68 cm	36.8	Cal/dolo	80	24109	75	36	85	12	0.4	49	66	7.5	24	3.4	26	3.3	0.3	2.1	0.4	1.5	0.4	3.4	0.9	8.7	88	2.0